minerals

MDPI

Article

Correlation of Neogene Oil and Paleogene Source Rocks in the Middle Huanghekou Sag, Bohai Bay Basin

Rui Hu, Xiaodong Lan * and Hao Liu

School of Ocean Sciences, China University of Geosciences, Beijing 100083, China; hurui200419@163.com (R.H.)
* Correspondence: lansecup@163.com

Abstract: Several billion-ton Neogene oil fields have been successfully discovered in the middle Huanghekou sag over the past few years. However, the source of the crude oil needs to be clarified, and the relevant oil-source correlation was less carried out. Six source rocks of the third member of the Paleocene Shahejie Formation (Es_3) from five wells and sixteen Neogene crude oil samples from nine wells in the middle Huanghekou sag were investigated for the oil-source correlation with the biomarkers and carbon and hydrogen isotopes of saturated hydrocarbon monomers. The distribution characteristics of n-alkanes, C_{19}/C_{23} ratio of tricyclic terpanes, long-chain tricyclic terpene ratios (ETR), C_{24} tetracyclic terpane to C_{26} tricyclic terpene, and distribution characteristics of conventional steranes suggest that the Es_3 parent material is of a mixed-source input from terrestrial higher plants and aquatic phytoplankton. The gammacerane to C_{30} hopane ratio is low, ranging from 0.094 to 0.134, with a mean value of 0.118; the Pr/Ph ratio is less than 1.5. The Neogene oils show the characteristics of a saturated hydrocarbon biomarker similar to Es_3. The carbon and hydrogen isotopes of saturated hydrocarbon monomers also corroborate the oil-source correlation from the depositional environment and parent material source, which characterize the low salinity of the water during the Es_3 sedimentary period, which was a brackish or a freshwater delta deposition under weak oxidation–weak reduction conditions. The parity dominance of CPI and OEP values (both greater than 1), higher ratios of Ts/Tm (1.174 to 1.383, mean 1.278) and the $C_{29}Ts/C_{29}$ norhopane, high values of diahopane and diasterane contents (C_{30}diaH/C_{30}H, C_{27}diaS/C_{27}S), and hopane and sterane isomerization parameters (%22S, %20S, %ββ) confirm that the Es_3 source rock samples are mature enough to provide crude oil for the middle Huanghekou sag. The biomarker characteristics of regional Neogene crude oil are significantly different from those of Es_4 source rocks in the surrounding depressions (sags), indicating the Es_4 strata's absence in the middle Huanghekou sag. Suitable traps need to be discovered around the hydrocarbon-generating center of the Es_3 source rock for oil and gas exploration in the future.

Keywords: source rock; biomarkers; middle Huanghekou sag; oil-source correlation

check for updates

Citation: Hu, R.; Lan, X.; Liu, H. Correlation of Neogene Oil and Paleogene Source Rocks in the Middle Huanghekou Sag, Bohai Bay Basin. *Minerals* **2023**, *13*, 586. https://doi.org/10.3390/min13050586

Academic Editor: Thomas Gentzis

Received: 10 March 2023
Revised: 16 April 2023
Accepted: 20 April 2023
Published: 22 April 2023

Copyright: © 2023 by the authors. Licensee MDPI, Basel, Switzerland. This article is an open access article distributed under the terms and conditions of the Creative Commons Attribution (CC BY) license (https://creativecommons.org/licenses/by/4.0/).

1. Introduction

With the increasing global consumption of fossil energy and the gradual depletion of onshore petroleum resources, unconventional oil and gas and offshore petroleum are receiving increasing and constant attention. The Bohai Bay Basin in eastern China is a Cenozoic rift basin [1–3], rich in petroleum resources, with proven oil reserves of approximately 13 billion tons and gas reserves of 351 billion m^3 [4–6]. Oil and gas exploration practices have shown that the petroleum distribution in the basin is closely related to the hydrocarbon-rich depressions (sags). Located in the southeastern part of the Bohai Bay Basin, the Huanghekou sag has a high potential for hydrocarbon exploration. However, it has undergone multiple phases of tectonic deformation, with both magmatic activity and complex tectonic styles [7,8]. In recent years, the Bozhong 19-6 condensate gas field with reserves of more than 100 billion m^3 was discovered in the northwest of the Huanghekou

sag [9,10], and several large and medium-sized Neogene fields, such as BZ34-9 and KL6-1, were successfully found in the middle of the sag [11–13].

Dozens of wells are drilled in the middle Huanghekou sag, with good oil and gas shows in the Neogene [14]. Therefore, the target of regional drilling wells is Neogene crude oil, so the exploration wells are generally not very deep. The deep strata below the third member of Paleocene Shahejie Formation (Es_3) have yet to be drilled through, and whether the fourth member of the Paleocene Shahejie Formation (Es_4) exists in the sag is still to be determined. Several sets of Paleocene source rocks developed in the Huanghekou sag, and the source of oil and gas is controversial, with few studies on the oil-source correlation. Combining regional geology and sedimentation, the oil-source correlation was carried out based on the organic geochemical biomarkers between the Neogene resource and the Paleocene reservoir rocks to determine the oil source, improving the geological understanding of the regional petroleum sources and the development of the deep strata, as well as providing information for regional hydrocarbon exploration in the future.

2. Regional Geology

The middle Huanghekou sag is located in the center of the Huanghekou sag, sandwiched between the Bonan Low uplift and the Laibei Low uplift, bounded by a strike–slip fault and central uplift in the west, and adjacent to the eastern Huanghekou sag in the east (Figure 1). The whole sag has the structural feature of "faulted in the north and onlap in the south" [15–17]. It can be divided into three sub-structural units: the northern steep slope belt, the central sub-depression, and the southern gentle slope belt.

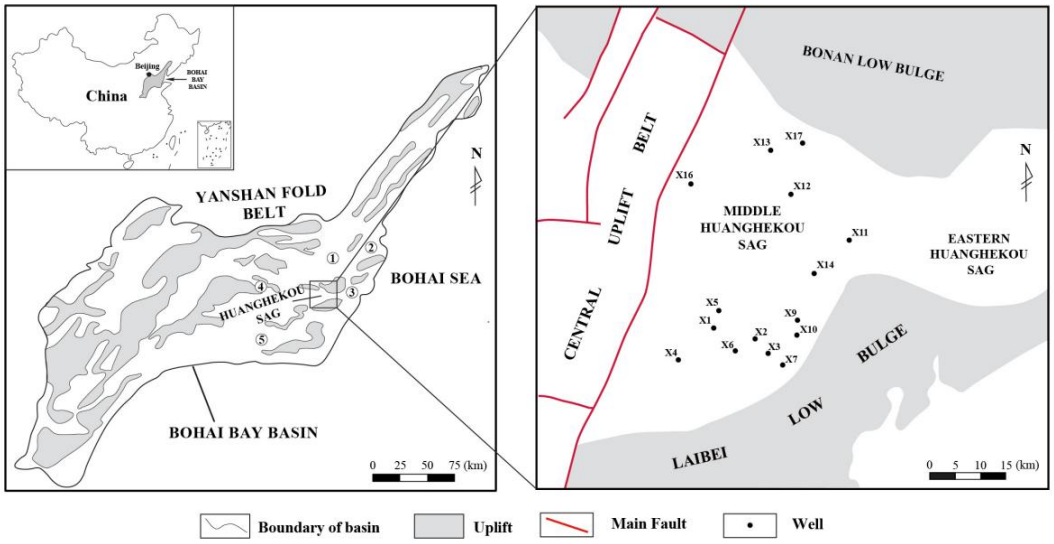


Figure 1. Location of the middle Huanghekou sag and well distribution. ① Bozhong sag; ② Bodong sag; ③ Miaoxi sag; ④ Chengbei sag; ⑤ Dongying sag.

Based on the regional drilling and seismic data, the Paleogene and Neogene strata in the Huanghekou sag are well developed (Figure 2). The Paleogene Shahejie Formation (Es) and Dongying Formation (Ed), the Neogene Guantao Formation (Ng) and Minghuazhen Formation (Nm), and the Quaternary Pingyuan Formation (Qp) were deposited in decreasing order of depth. According to the basin characteristics and surrounding strata, the Shahejie Formation can be subdivided into four members, namely, Es_1, Es_2, Es_3, and Es_4, from top to base, and the Dongying Formation can also be subdivided into three members from top to bottom, namely, Ed_1, Ed_2, and Ed_3. The lithology of the middle sag sedimentary strata is mainly sand and mudstone. The Paleogene sedimentary system is mainly delta facies and coastal shallow lake to semi-deep lake. However, the Neogene sedimentary system is mainly fluvial facies and shallow water delta facies [18]. There are several sets of high-quality sand-body reservoirs, such as the Paleogene Shahejie and Dongying Forma-

tions, and the Neogene Guantao and Minghuazhen Formations, and oil and gas are mainly enriched in the shallow Neogene Guantao and Minghuazhen Formations. The potential argillaceous source rocks in the sag include the Es_4, Es_3, Es_1, and Ed_3 formations. However, the source rocks in and above Es_1 and Es_2 in the Huanghekou sag are shallowly buried and have not reached the hydrocarbon generation threshold [19]. Therefore, the interference of the hydrocarbon supply from these source rocks is excluded, and the lower strata of the Shahejie Formation are thought to be the regional source rocks.

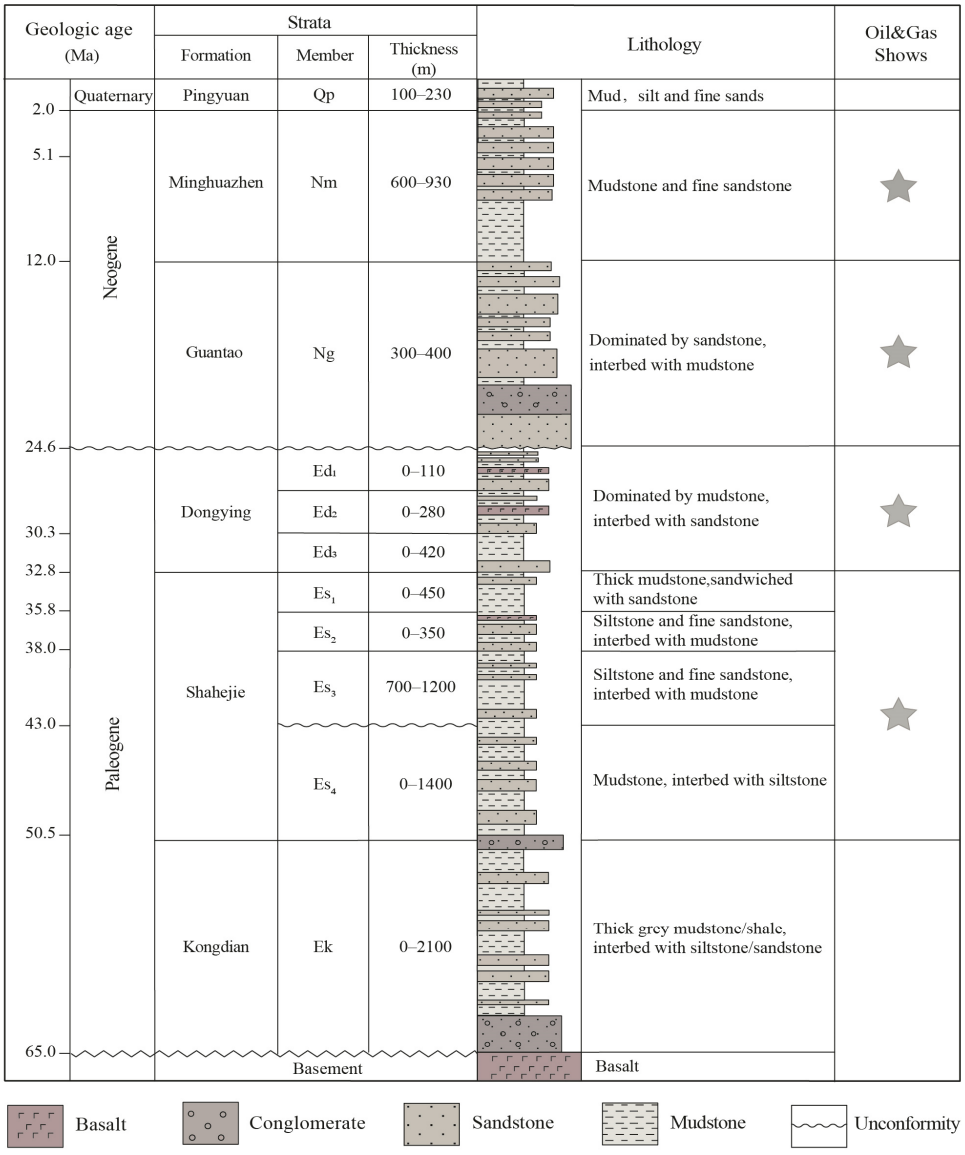


Figure 2. Lithologic composite histogram of the Huanghekou sag.

3. Samples and Methods

The well distribution in this paper is shown in Figure 1. The 6 Es_3 samples of drilled cuttings from 5 wells were numbered S1, S2, S3, S4, S5, and S6 (Table 1). Crude oil samples were collected from the Minghuazhen and Guantao Formations, with a total of 16 samples from 9 wells, including 12 from the Minghuazhen Formation and 4 from the Guantao Formation, numbered as O1~O16, and were taken from the X1, X3, X4, X7~X10, and X13 wells (Table 2). Most samples were concentrated in the south gentle slope belt, while a small amount of crude oil samples was found in the north steep slope belt. Organic solvent, saturated hydrocarbon gas chromatography–mass spectrometry (GC-MS), and hydrocarbon isotope experiments were conducted on source rock and crude oil samples.

Table 1. GC parameters of source rocks and crude oils in the middle Huanghekou sag.

Sample	Strata	Well	Pr/Ph	Pr/*n*-C_{17}	Ph/*n*-C_{18}	CPI	OEP	Nmax	*n*-C_{21}/*n*-C_{22}^{+}	*n*-C_{21} + *n*-C_{22}/*n*-C_{28} + *n*-C_{29}	TAR	2*n*-C_{17}/(*n*-C_{23} + *n*-C_{25})
S1	Es_3	X1	1.171	0.804	0.292	1.127	1.318	23	0.463	1.959	1.712	0.204
S2	Es_3	X2	1.223	0.497	0.281	1.056	1.138	25	0.110	0.533	7.123	0.087
S3	Es_3	X4	1.043	0.621	0.433	1.054	1.084	23	0.441	1.572	1.468	0.404
S4	Es_3	X5	1.476	1.249	0.794	1.119	1.279	25	0.458	1.167	1.658	0.571
S5	Es_3	X6	1.052	0.422	0.318	1.071	1.120	25	0.231	0.797	2.873	0.243
S6	Es_3	X6	1.086	0.371	0.466	1.075	1.108	25	0.420	0.848	1.446	0.625
O1	Nm	X1	0.896	0.394	0.403	1.089	1.045	23	0.643	1.795	0.874	0.754
O2	Nm	X1	0.902	0.369	0.382	1.099	1.053	23	0.710	1.928	0.736	0.752
O3	Nm	X3	0.949	1.950	1.495	1.109	1.148	25	0.303	1.249	2.470	0.260
O4	Nm	X3	0.918	1.988	1.707	1.086	1.117	25	0.274	1.093	2.896	0.257
O5	Nm	X4	0.866	2.454	2.207	1.069	1.12	25	0.147	0.645	7.093	0.118
O6	Nm	X7	0.904	2.436	2.214	1.117	1.191	25	0.286	1.077	2.572	0.299
O7	Nm	X7	0.847	2.485	2.364	1.093	1.173	25	0.224	0.835	3.602	0.258
O8	Nm	X7	0.859	2.265	2.114	1.104	1.184	25	0.278	1.026	2.665	0.302
O9	Nm	X9	1.045	3.026	2.006	1.132	1.301	25	0.209	0.870	3.816	0.202
O10	Nm	X10	0.893	0.542	0.545	1.083	1.052	23	0.576	1.810	1.001	0.665
O11	Nm	X10	0.826	1.279	1.146	1.084	1.12	25	0.376	1.369	1.845	0.379
O12	Nm	X13	1.003	4.795	3.718	1.171	1.526	25	0.320	1.083	2.194	0.264
O13	Ng	X2	0.952	1.596	1.978	1.085	1.203	25	0.297	1.243	1.918	0.398
O14	Ng	X8	0.815	0.521	0.528	1.089	1.118	25	0.424	1.388	1.544	0.452
O15	Ng	X8	0.852	0.510	0.534	1.051	1.025	23	0.463	1.360	1.381	0.573
O16	Ng	X10	1.146	6.281	7.782	1.085	1.163	25	0.152	0.961	8.461	0.120

Pr/Ph = pristine/phytane ratio; Pr/*n*-C_{17} = pristane to *n*-C_{17} alkane ratio; Ph/*n*-C_{18} = phytane to *n*-C_{18} alkane ratio; OEP = (*n*-C(Nmax-2) + 6 × *n*-CNmax + *n*-C(Nmax+2))/(4 × *n*-C(Nmax–1) + *n*-C(Nmax+1)); Nmax = max peak carbon number of the *n*-alkanes; CPI = 0.5×(*n*-C25 + *n*-C27 + *n*-C29 + *n*-C31 + *n*-C33) × [1/(*n*-C24 + *n*-C26 + *n*-C28 + *n*-C30 + *n*-C32) + 1/(*n*-C26 + *n*-C28 + *n*-C30 + *n*-C32 + *n*-C34)]; TAR = (*n*-C27 + n-C29 + *n*-C31)/(*n*-C15 + *n*-C17 + *n*-C19).

Table 2. Saturated hydrocarbon related parameters between source rocks and crude oils in the middle Huanghekou sag.

Sample	Strata	Well	Ga/C_{30}H	Ol/C_{30}H	Ts/Tm	C_{30}diaH/C_{30}H	C_{29}Ts/C_{29}H	%22S	C_{19}TT/$_{C23}$TT	C_{22}TT/C_{21}TT	C_{24}TT/C_{23}TT	C_{24}Te/C_{26}TT	ETR	C_{27}S	C_{28}S	C_{29}S	C_{27}diaS/C_{27}S	%20S	%ββ
S1	Es_3	X1	0.094	0.082	1.245	0.100	0.473	0.590	0.168	0.251	0.583	2.571	0.431	0.386	0.112	0.502	0.533	0.487	0.375
S2	Es_3	X2	0.134	0.095	1.319	0.084	0.439	0.612	0.112	0.426	0.642	0.371	0.442	0.419	0.200	0.381	0.399	0.389	0.396
S3	Es_3	X4	0.131	0.098	1.358	0.098	0.349	0.591	0.145	0.282	0.715	0.691	0.401	0.362	0.216	0.423	0.194	0.395	0.435
S4	Es_3	X5	0.104	0.097	1.215	0.085	0.342	0.590	0.214	0.237	0.578	0.754	0.439	0.450	0.169	0.381	0.433	0.365	0.369
S5	Es_3	X6	0.124	0.103	1.278	0.105	0.358	0.593	0.163	0.250	0.654	0.885	0.486	0.356	0.204	0.440	0.201	0.409	0.450
S6	Es_3	X6	0.120	0.095	1.194	0.091	0.270	0.599	0.252	0.241	0.666	0.971	0.440	0.345	0.206	0.449	0.149	0.389	0.417
O1	Nm	X1	0.154	0.071	1.174	0.078	0.406	0.590	0.215	0.270	0.623	0.686	0.393	0.389	0.202	0.408	0.187	0.416	0.442
O2	Nm	X1	0.167	0.075	1.186	0.082	0.406	0.596	0.212	0.276	0.586	0.700	0.387	0.375	0.211	0.414	0.174	0.440	0.427
O3	Nm	X3	0.122	0.088	1.326	0.094	0.389	0.603	0.276	0.291	0.639	0.830	0.409	0.406	0.232	0.362	0.216	0.417	0.460
O4	Nm	X3	0.120	0.100	1.249	0.088	0.352	0.598	0.249	0.273	0.659	0.737	0.443	0.407	0.221	0.372	0.237	0.419	0.447
O5	Nm	X4	0.129	0.077	1.242	0.087	0.385	0.591	0.194	0.269	0.709	0.680	0.400	0.403	0.212	0.385	0.240	0.411	0.424
O6	Nm	X7	0.122	0.081	1.365	0.092	0.451	0.594	0.343	0.261	0.702	0.679	0.438	0.389	0.206	0.406	0.262	0.420	0.435
O7	Nm	X7	0.125	0.083	1.325	0.089	0.450	0.590	0.288	0.270	0.728	0.677	0.438	0.389	0.211	0.401	0.246	0.433	0.435
O8	Nm	X7	0.123	0.082	1.382	0.094	0.446	0.592	0.301	0.266	0.713	0.666	0.440	0.393	0.208	0.399	0.265	0.427	0.423
O9	Nm	X9	0.114	0.081	1.304	0.086	0.430	0.591	0.255	0.278	0.740	0.679	0.446	0.389	0.210	0.400	0.256	0.439	0.432
O10	Nm	X10	0.124	0.088	1.255	0.086	0.381	0.592	0.236	0.262	0.675	0.670	0.444	0.405	0.221	0.374	0.261	0.439	0.452
O11	Nm	X10	0.118	0.081	1.313	0.110	0.404	0.592	0.261	0.252	0.686	0.691	0.436	0.402	0.225	0.373	0.274	0.455	0.451
O12	Nm	X13	0.138	0.083	1.383	0.101	0.475	0.576	0.359	0.241	0.716	2.548	0.329	0.424	0.207	0.403	0.258	0.451	0.439
O13	Ng	X2	0.092	0.092	1.187	0.084	0.370	0.588	0.156	0.285	0.622	0.811	0.402	0.404	0.224	0.373	0.244	0.459	0.469
O14	Ng	X8	0.124	0.076	1.331	0.086	0.438	0.585	0.300	0.261	0.889	0.803	0.305	0.425	0.217	0.359	0.206	0.630	0.447
O15	Ng	X8	0.118	0.065	1.245	0.089	0.409	0.589	0.286	0.229	0.810	0.868	0.291	0.398	0.209	0.393	0.219	0.405	0.442
O16	Ng	X10	0.084	0.094	1.175	0.080	0.332	0.590	0.260	0.265	0.736	0.710	0.484	0.385	0.213	0.401	0.322	0.439	0.409

%22S = 22S/(22S + 22R) ratio of C_{31} to C_{35} homohopanes; ETR = (C_{28}TT + C_{29}TT)/(C_{28}TT + C_{29}TT + Ts) ratio; C_{27}S, C_{28}S, and C_{29}S = percentages of C_{27}, C_{28}, and C_{29} of regular Sterane; %20S = 20S/(20S + 20R) ratio of $C_{29}\alpha\alpha\alpha$ sterane; %ββ = ββ/(αα + ββ) of C_{29} regular sterane.

Before GC and GC-MS experimental analysis, the extraction of soluble organic matter from the source rock samples was carried out. After removing surface contamination, the samples were cleaned and dried, then ground to 200 mesh. The Soxhlet extraction method was used to pack a proper amount of the crushed sample in a filter paper cylinder into the extractor, add 300 mL dichloromethane into the bottom flask and add several copper pieces for desulfurization, and then install the extractor and flask containing the sample on the support. After turning on the power and starting the extraction of organic matter, the extraction was continued for 24 h. The organic matter extraction solution was precipitated with petroleum ether for 48 h, and the filtrate part according to the principle of solid–liquid adsorption balance, through the silica gel alumina chromatography column, using solvents of different polarity, the saturated hydrocarbon, aromatic hydrocarbon, and colloidal group (non-hydrocarbon) respectively leaching, volatile solvent, weighing constant weight, the content of each component in soluble organic matter or crude oil. Then, the saturated hydrocarbon fractions were determined by GC and GC/MS.

GC and GC-MS experimental analysis of source rock extracts and crude oils was performed and completed at CNOOC Bohai Experimental Center, Tianjin, China.

The gas chromatograph (GC) used for saturated hydrocarbon analysis was a HP-6890 chromatograph with a PONA fused silica column (60 m × 0.20 mm × 0.5 μm). The initial temperature was held at 35 °C for 5 min and first programmed to 80 °C (2 °C/min), then to 300 °C (4 °C/min), and held for 30 min. GC-MS of saturated hydrocarbon fractions was performed on a Thermo Fisher Trace-DSQII instrument using an HP-5MS fused silica column (60 m × 0.25 mm × 0.25 μm). The initial temperature was maintained at 50 °C/min and programmed to 100 °C at 15 °C/min, then to 200 °C at 2 °C/min, followed by 315 °C at 1 °C/min, and held for 20 min. The flow rate of the carrier gas was 1 mL/min.

In this study, three crude oil samples were selected to test hydrocarbon isotopes of saturated hydrocarbon monomers; the sample numbers are O3, O4, and O14. The experiments were conducted at the Oil and Gas Resources and Exploration State Key Laboratory, China University of Petroleum (Beijing). The n-alkanes and isoparaffins were separated by the5A molecular sieve adsorption separation method, and GC-IR-MS and GC-TC-IR-MS, respectively, measured the obtained n-alkanes. A Micromass Isoprim isotope mass spectrometer coupled with HP6890 gas chromatography analyzed the monomeric hydrocarbon carbon isotopes. The chromatographic column was a phenyl-methyl-silicone stationary phase capillary column (60 m × 0.25 mm × 0.25 μm), and the ramp-up procedure of the gas chromatography was as follows: 50 °C for 1 min, ramped up to 310 °C at 3 °C/min, constant temperature for 30 min, Helium (He) carrier gas, constant flow mode, flow rate 1.0 mL/min. The deviation of repeat analysis test data was less than 0.3‰. The isotopic composition of monomeric hydrocarbon hydrogen was determined using a Delta-Plus XL chromatography-isotope ratio mass spectrometer with a DB-5MS flexible capillary column (30 m × 0.32 mm × 0.25 μm) at a starting temperature of 50 °C, ramped up to 90 °C at a rate of 15 °C/min and constant temperature for 1 min, then ramped up to 290 °C at 6 °C/min and constant temperature for 20 min. The effluent was heated to 1400 °C through the oxidation tube, and the organic H was converted to H_2^+ and entered the isotope ratio mass spectrometer. The H_3^+ factor of the instrument was measured once after each sample (3 or 4 injections) to ensure that the H_3^+ factor was essentially constant throughout the analysis; all hydrogen isotope values were the average of more than 3 measurements.

4. Results

4.1. Saturated Hydrocarbon GC and GC-MS

In the saturated hydrocarbon chromatogram, the GC patterns of the samples can show the differences in sedimentary environment and organic matter sources (Figure 3), and *m/z* 85 is usually used to express the distribution-related ratio parameters of n-alkanes in the total ion flow, as shown in Table 1 (the data were calculated by peak area). The CPI and OEP of the Es_3 source rock samples ranged from 1.054 to 1.127 and 1.084 to 1.318, respectively, with mean values of 1.084 and 1.175, respectively, showing some parity dominance. The CPI

and OEP of the crude oil samples ranged from 1.051 to 1.171 and 1.025 to 1.526, respectively, with mean values of 1.097 and 1.159, respectively, also showing some parity dominance. The max peak carbon number of the Es_3 samples ranged from n-C_{23} to n-C_{25}; TAR ranged from 1.446 to 7.123, with a mean value of 2.713; n-C_{21}-/n-C_{22}^+ ranged from 0.110 to 0.463, with a mean value of 0.354; (n-C_{21} + n-C_{22})/(n-C_{28} + n-C_{29}) ranged from 0.533 to 1.959, with 1.146 on average; and 2n-C_{17}/(n-C_{23} + n-C_{25}) ranged from 0.087 to 0.625, with an average of 0.356. Similar to the range of the Es_3 samples, the max peak carbon number of the crude oil samples ranged from 23 to 25, with TAR ranging from 0.736 to 8.461, and the average was 2.817; n-C_{21}-/n-C_{22}^+ ranged from 0.147 to 0.710, with a mean value of 0.355; (n-C_{21} + n-C_{22})/(n-C_{28} + n-C_{29}) ranged from 0.645 to 1.928, with 1.233 on average; and 2n-C_{17}/(n-C_{23} + n-C_{25}) ranged from 0.118 to 0.754, with an average of 0.378. Pr/Ph ranged from 1.043 to 1.476, with a mean value of 1.175, and Pr/n-C_{17} and Ph/n-C_{18} ranged from 0.371 to 1.249 and 0.281 to 0.794, respectively, with a mean value of 0.661 and 0.431, respectively. The Pr/Ph of the crude oil samples ranged from 0.815 to 1.146, with a mean value of 0.917.

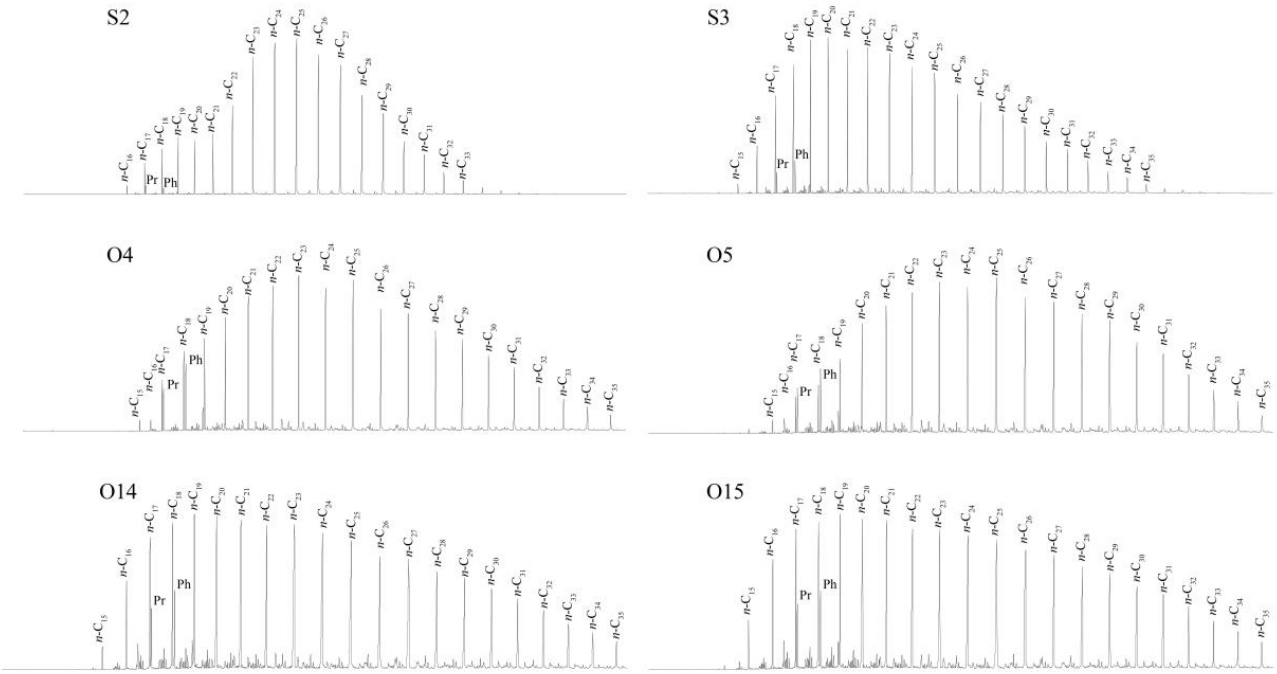


Figure 3. GC characteristics of saturated hydrocarbon for typical source rocks and oils in the middle Huanghekou sag. In addition to the n-alkane distribution, a typical GC-MS fragmentation plot (Figure 4) shows the biomarker distribution of terpene and hopane (*m/z* 191) and sterane (*m/z* 217), and the peak area ratios calculated from the integrals are given in Table 2 (the data were calculated by peak area).

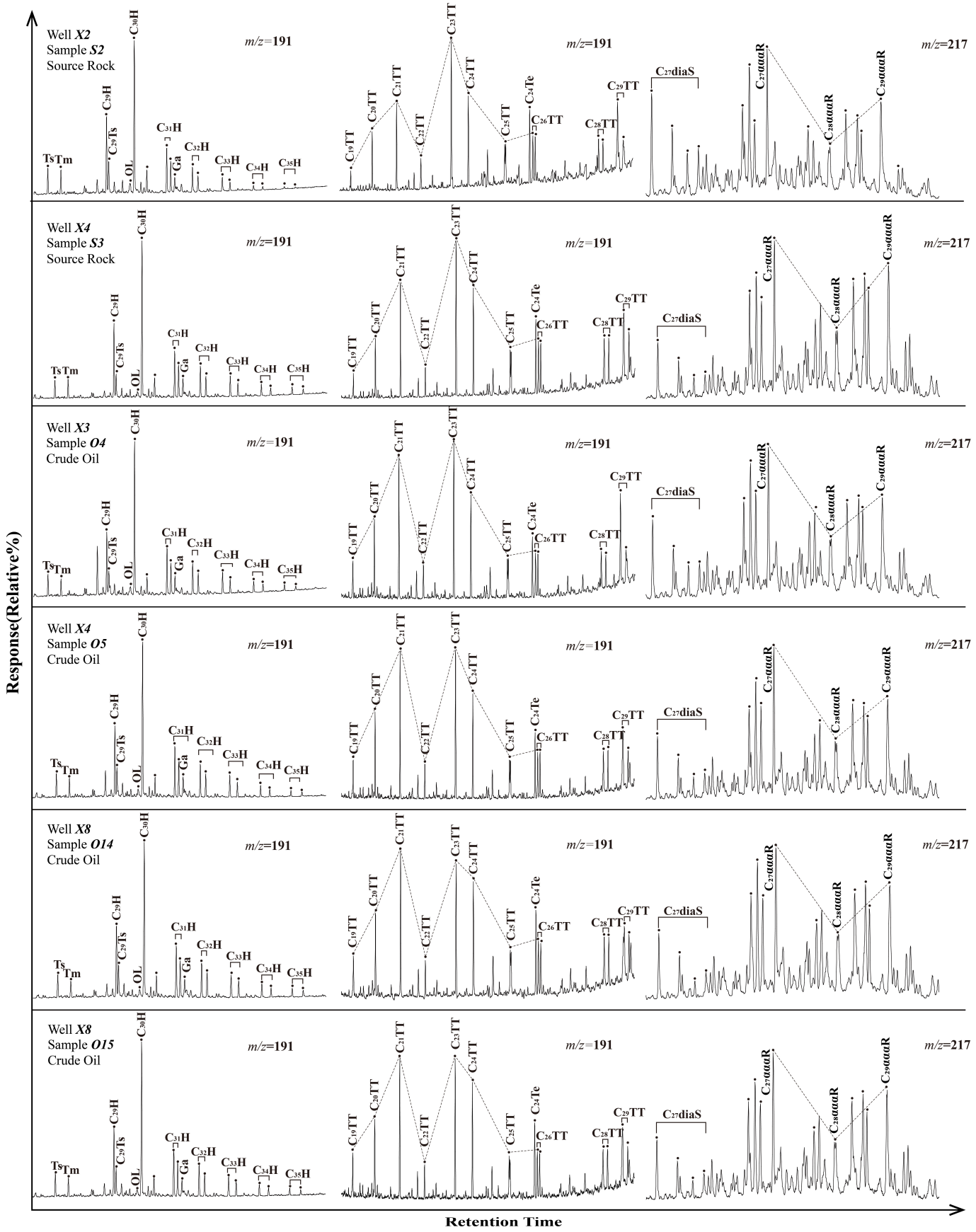


Figure 4. GC-MS characteristics of saturated hydrocarbon for typical source rocks and oils in the middle Huanghekou sag.

The *m/z* 191 mass spectra show the distribution of hopane and terpane in representative source rock and crude oil samples. As seen in Figure 3, the samples have a lower content of gammacerane (Ga), oleanane (Ol), and C_{35} homohopane, and relatively higher Ts and C_{29} 18α-30-norneohopane (C_{29}Ts) content. The values of Ga/C_{30}H in the Es_3 source rocks range from 0.094 to 0.134, with a mean value of 0.118; the Ol/C_{30}H ratios range from 0.082 to 0.103, with 0.095 on average; the ratio of Ts to Tm ranges from 1.194 to 1.358, with 1.268 on average; and the ratio of C_{29}Ts to C_{29} hopane (C_{29}H) ranges from 0.270 to 0.473, and the average is 0.372. The crude oil is similar to the source rock in numerical range. The values of Ga/C_{30}H ranged from 0.084 to 0.167, with an average value of 0.124; the values of Ol/C_{30}H ranged from 0.065 to 0.100, with an average of 0.082; the ratio of Ts to Tm ranged from 1.174 to 1.383, with 1.278 on average; and the ratio of C_{29}Ts to C_{29}H ranged from 0.332 to 0.475, with a mean value of 0.408.

As for the tricyclic terpenes, the overall content of C_{19} Tricyclic terpane (C_{19}TT) was low, and the content of C_{23} tricyclic terpane (C_{23}TT) was high in the Es_3 source rocks, with the C_{19}TT/C_{23}TT ratio ranging from 0.112 to 0.252 with 0.176 on average. The C_{24} tetracyclic terpane (C_{24}Te) has higher content, and its ratio to C_{26} tricyclic terpane (C_{26}TT) ranged from 0.371 to 2.571, with a mean value of 1.040. The C_{28} tricyclic terpane (C_{28}TT) and C_{29} tricyclic terpane (C_{29}TT) content of long-chain tricyclic terpenes was relatively high; the ETR values ranged from 0.401 to 0.486, with an average value of 0.440. The values of C_{19}TT/C_{23}TT for the crude oil samples ranged from 0.156 to 0.359, with a mean value of 0.262; the C_{24}Te/C_{26}TT ratio ranged from 0.666 to 2.548, with 0.840 on average; and the values of ETR ranged from 0.291 to 0.484, with a mean value of 0.405.

Among the *m/z* 217 steranes, the C_{27} sterane (C_{27}S) content of the Es_3 source rock samples was higher, ranging from 0.345 to 0.450, with an average of 0.386; the C_{28} sterane (C_{28}S) content was lower, ranging from 0.112 to 0.216, with a mean value of 0.184; and the C_{29} sterane (C_{29}S) content was relatively higher, ranging from 0.381 to 0.502, and the average was 0.429. The overall distribution of three steranes (Figure 4) is like a "V" shape of lower C_{28}S and higher C_{27}S and C_{29}S. Similar to the Es_3 samples, the C_{28}S content of the crude oil samples was lower, ranging from 0.202 to 0.232, with an average value of 0.214; the C_{27}S and C_{29}S contents were higher, like a "V" shape, ranging from 0.375 to 0.425 and 0.359 to 0.414, respectively, with the averages 0.399 and 0.389, respectively. The sample C_{27} diasterane (C_{27}diaS) contents were high, and the relative abundance of isomerized steranes was relatively high, as well. The Es_3 source rock values of C_{27}diaS/C_{27}S ranged from 0.149 to 0.533, with an average value of 0.318, and the values of C_{27}diaS/C_{27}S of the crude oil samples ranged from 0.174 to 0.322, with 0.242 on average.

4.2. Carbon and Hydrogen Isotopes of Saturated Hydrocarbon Monomers of Crude Oil

Based on the test results (Tables 3 and 4), the carbon isotope distribution of the saturated hydrocarbon monomers for the crude oil samples shows a pattern of higher on both sides and lower in the middle, the left side of the carbon isotope curve is slightly higher than the right side, and the values range from −32.1‰ to −24.3‰ overall. However, the distribution curve of hydrogen isotopes is relatively flat, with no apparent fluctuation overall, ranging from −210.8‰ to −121.1‰, in which the right side is slightly higher than the left.

Table 3. Carbon isotope data of saturated hydrocarbon monomers from Cenozoic crude oils (Unit: ‰).

Sample	*n*-C_{16}	*n*-C_{17}	*n*-C_{18}	*n*-C_{19}	*n*-C_{20}	*n*-C_{21}	*n*-C_{22}	*n*-C_{23}	*n*-C_{24}	*n*-C_{25}	*n*-C_{26}	*n*-C_{27}	*n*-C_{28}	*n*-C_{29}	*n*-C_{30}	*n*-C_{31}	*n*-C_{32}	*n*-C_{33}	*n*-C_{34}
O3	—	—	−26.7	−27.9	−27.7	−27.8	−28.1	−28.8	−28.1	−28.7	−32.1	−31.8	−29.5	−29.7	−28.4	−27.8	−26.1	−27.1	−26.6
O4	−25.7	−26.1	−26.6	−26.0	−26.4	−27.2	−27.5	−28.2	−28.2	−28.7	−29.6	−29.9	−29.5	−29.6	−29.4	−27.6	−26.3	−25.7	−26.1
O14	−25.7	−26.1	−26.6	−26.0	−26.4	−27.2	−27.5	−28.2	−28.2	−28.7	−29.6	−29.9	−29.5	−29.6	−29.4	−27.6	−26.3	—	—

"—" means not detected.

Table 4. Hydrogen isotope data of saturated hydrocarbon monomers from crude oil samples (Unit: ‰).

Sample	*n*-C_{16}	*n*-C_{17}	*n*-C_{18}	*n*-C_{19}	*n*-C_{20}	*n*-C_{21}	*n*-C_{22}	*n*-C_{23}	*n*-C_{24}	*n*-C_{25}	*n*-C_{26}	*n*-C_{27}	*n*-C_{28}	*n*-C_{29}	*n*-C_{30}
O3	−121.1	−179.9	−172.8	−170.8	−162.5	−152.6	−161.6	−154.7	−150.3	−156.6	−136.0	−150.7	−148.3	−146.4	−150.4
O4	—	—	−166.3	−184.7	−183.8	−171.5	−180.4	−161.1	−153.7	−172.1	−155.2	−160.7	−156.7	−175.7	−148.3
O14	−210.8	−177.4	−178.1	−165.8	−166.4	−165.0	−175.6	−174.7	−175.5	−193.0	−160.3	−172.2	−161.4	−180.5	−174.8

"—" means not detected.

5. Discussions

5.1. Correlation between Regional Crude Oil and Es_3 Source Rock

Saturated hydrocarbon biomarker parameters can be used to reflect the sedimentary environment, parent material source, and thermal maturity [20,21]. In addition to the biomarkers, the carbon isotope of saturated hydrocarbon monomers can also reflect the sedimentary environment of source rocks and crude oils, and is less affected by secondary geological processes, such as maturity, biodegradation, and hydrocarbon migration [22–24]. The hydrogen isotope composition is closely related to the parent material's organic matter and thermal evolution degree, and is also affected by the salinity of the sedimentary environment water [25].

5.1.1. Sedimentary Environment Comparison

The distribution characteristics of pristane (Pr) and phytane (Ph) can be used to reflect the sedimentary environment of source rocks [26]. Generally speaking, it is a strong reducing sedimentary environment when the Pr/Ph ratio is less than 0.5, a reducing environment with Pr/Ph ratio 0.5~1.0, a weak reduction–weak oxidation environment with Pr/Ph 1.0~2.0, and a partially oxidizing environment with Pr/Ph more than 2.0 [27,28]. According to the test results, the Es_3 source rocks deposited in a weak reduction–oxidation environment, and Pr/*n*-C_{17} correlated with Ph/*n*-C_{18} [29,30] can also intuitively show that the Es_3 sedimentary environment was weak reduction–weak oxidation (Figure 5) and maybe a delta environment entering the lake. Therefore, it presents alternating periods of reducing and oxidizing conditions. The reducibility of crude oil samples is slightly higher than that of the Es_3 source rock, and the correlation between them is good.

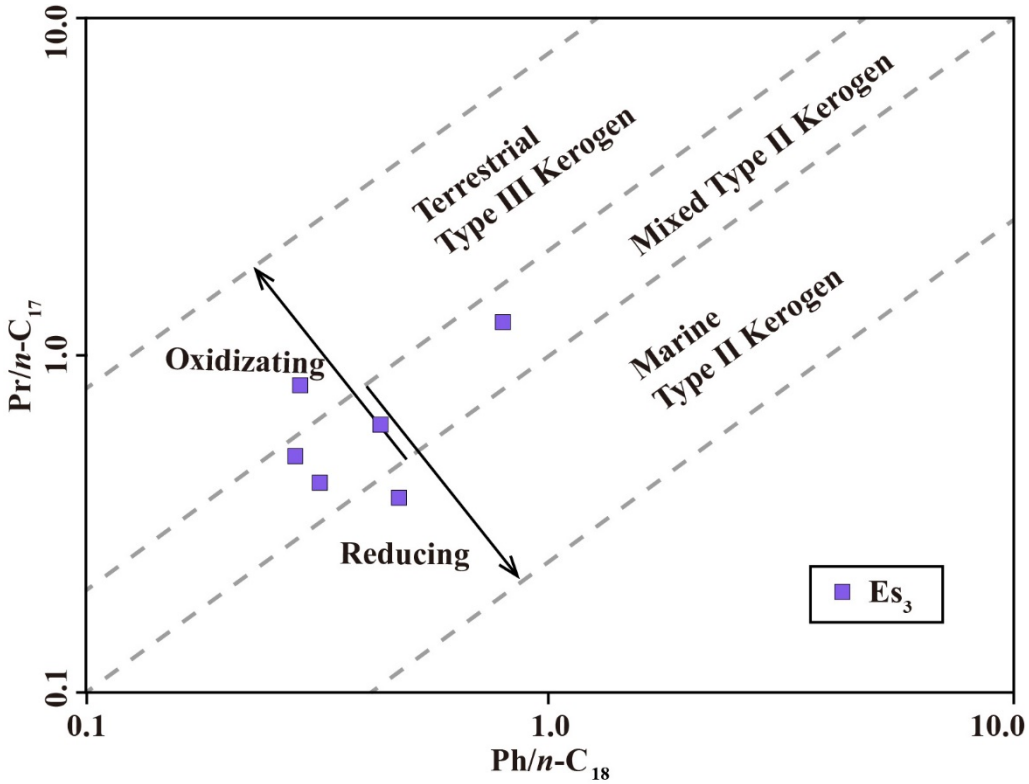


Figure 5. Relationship between Pr/*n*-C_{17} and Ph/*n*-C_{18} for extracted source rocks.

It is important that, regardless, the depositional environment oils and source rock extracts plot in a broadly similar range. The content of Ga is related to the water salinity and stratification, and it can be used to characterize the sedimentary environment with strong reduction and hypersalinity [31]. The Ga/C_{30}H ratio of Es_3 source rock samples is

low, with an average value of 0.118, indicating that the Es_3 sedimentary environment is a low-salinity delta. The crude oil samples also show this $Ga/C_{30}H$ characteristic, as shown in Figure 6. Except for Ga, the ETR and $C_{27}diaS/C_{27}S$ reflect the salinity of the sedimentary environment [32,33]. ETR is positively proportional to the Ga, and $C_{27}diaS/C_{27}S$ is inversely proportional to the Ga, which also reflects that the Es_3 source rocks deposited in a relatively low-salinity, brackish-to-freshwater environment. Crude oil also contains relevant parameters that show these characteristics have a good correlation with crude oil.

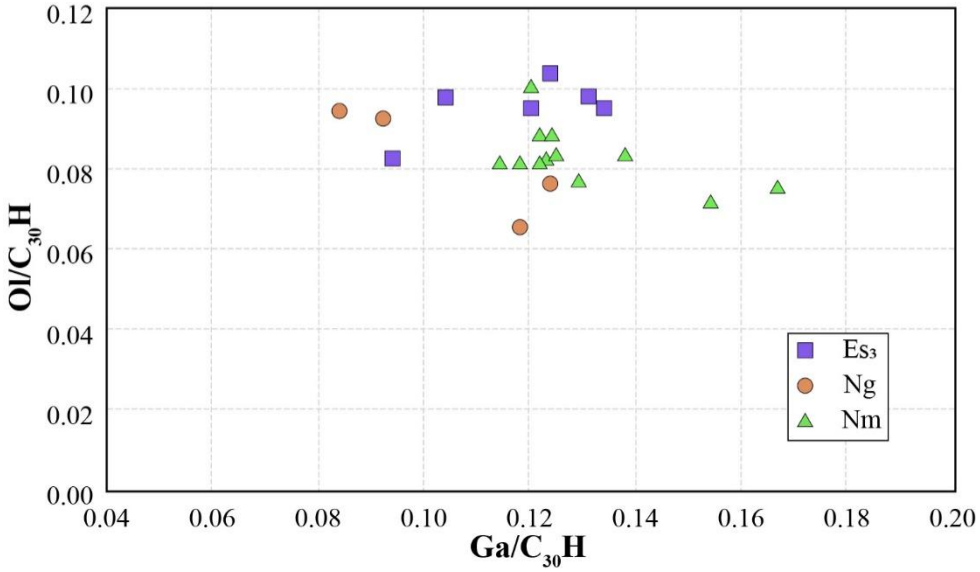


Figure 6. Relationship between $Ga/C_{30}H$ and $Ol/C_{30}H$ of source rocks and oils.

$C_{23}TT$ is abundant in marine facies and salt lake facies [34]. The ratios of $C_{24}/C_{23}TT$ and $C_{22}/C_{21}TT$ help to determine the source of crude oil [35]; as shown in Figure 7, the Es_3 source rock samples are located between lacustrine shale and Marine shale, and show the brackish/freshwater sedimentary characteristics. The crude oil samples are roughly distributed in a similar area, basically with the Es_3 source rocks.

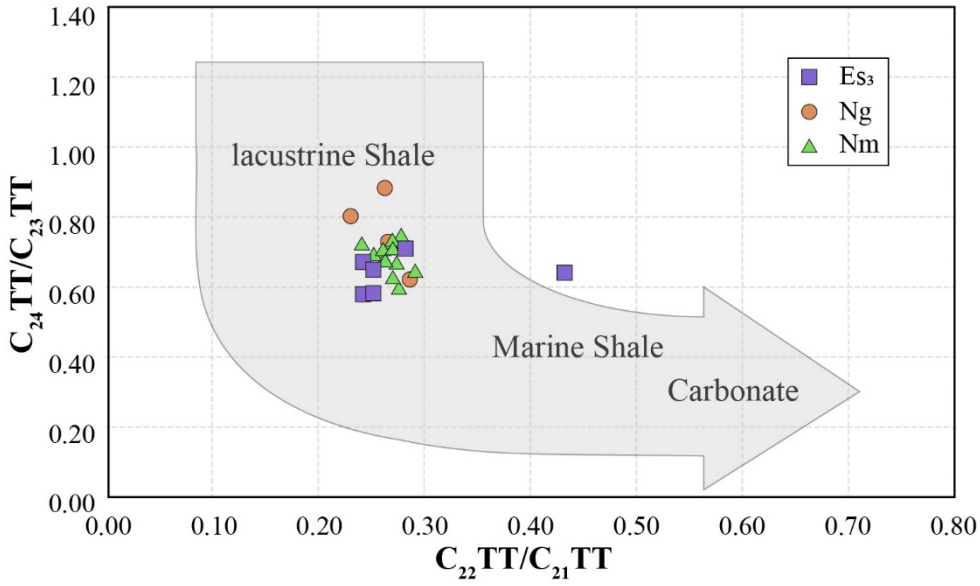


Figure 7. Sedimentary environment indicated by the ratios of $C_{24}TT/C_{23}TT$ and $C_{22}TT/C_{21}TT$.

The −28‰ of the carbon isotope value of saturated hydrocarbon monomers is used to divide salt water and fresh water environments [36,37]. In Figure 8, it can be seen that there is a certain similarity between three crude oils, indicating a high correlation between the crude oils, and the sedimentary environment also has a certain similarity. The Es_3 formation in the study area is brackish or a freshwater delta facies deposition, which is highly consistent [36] with the carbon isotope values. In addition, previous studies in neighboring areas found that the crude oil generated from the Es_3 source rock has relatively heavy carbon isotopes and shows a double-peak curve with the max carbon peaks of *n*-C_{15} and *n*-C_{32} [37]. Although there is a lack of carbon isotope data lower than *n*-C_{15} in the study samples, the curve trend shows that there is a high possibility of a max carbon peak of *n*-C_{15}. There is a max peak carbon of *n*-C_{32} (Figure 8), which is basically consistent with previous research results [36], indicating that the crude oil samples in the study area are more likely to be derived from the Es_3 source rock.

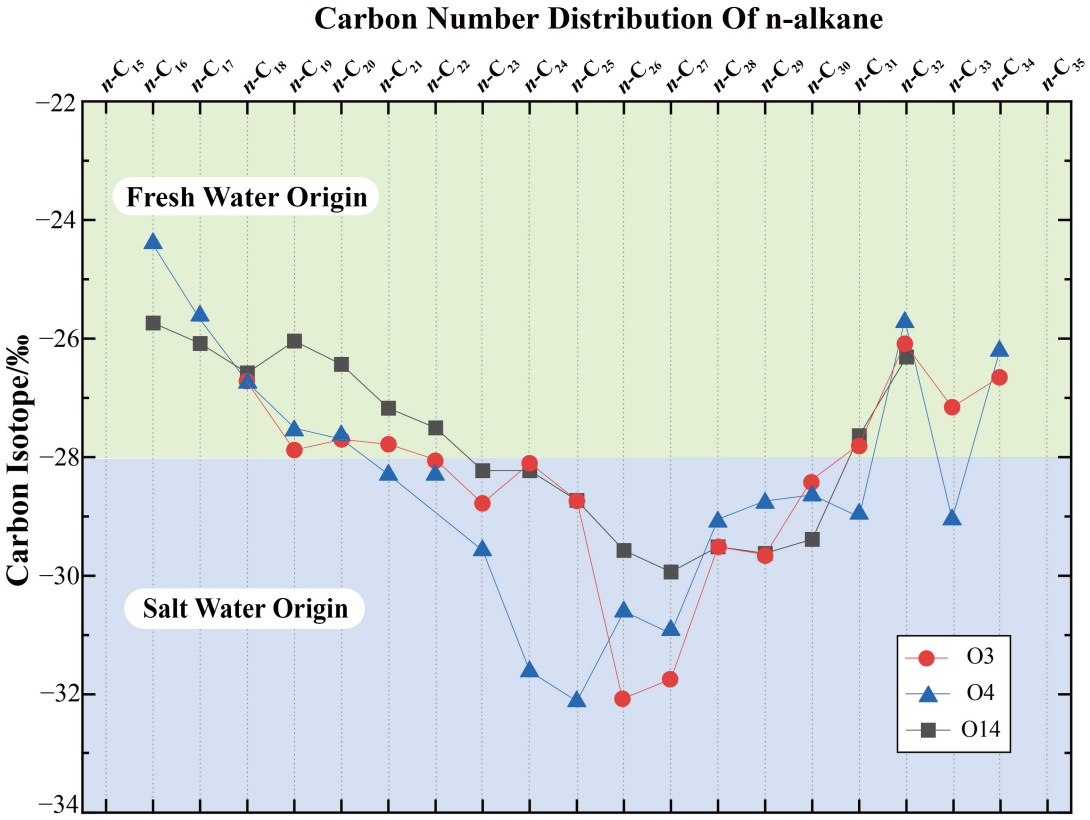


Figure 8. Carbon isotope compositions of individual alkanes from the Cenozoic crude oils. The green area ranges from −28 to −22 represents freshwater origin and the blue area ranges from −34 to −28 represents salt water origin.

Figure 9 shows the hydrogen isotope distribution of the crude oil samples in the study area. By observing their distribution curves, it can be observed that these crude oil samples are roughly distributed in one range and have the same trend, showing a good correlation and indicating that their sources may be similar. The previous study on the hydrogen isotopes of saturated hydrocarbon monomers in neighboring areas showed that the hydrogen isotope values of n-alkanes in the Es_3 formation range from −212‰ to −134‰, and between −161‰ and −111‰ for the Es_4 formation [38]. In comparison, the distribution of the hydrogen isotopes of the crude oils in the study area is similar to that of the Es_3 in the surrounding area. In addition, the hydrogen isotope curves of the crude oils are distributed between the saline and the freshwater sedimentary environment, showing that the parent material of the crude oils is mixed, and maybe more likely derived from the delta deposit rather than from the Es_3 source rocks in the study area.

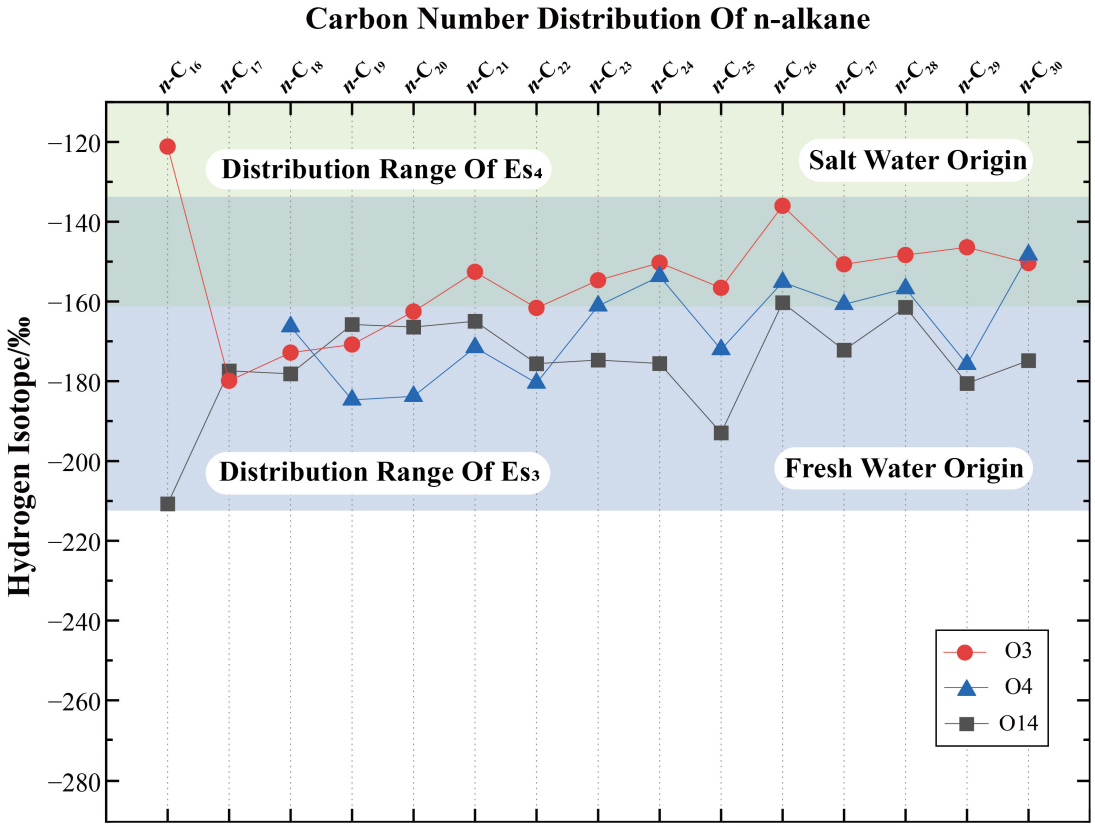


Figure 9. Hydrogen isotope compositions of individual alkanes from three oil samples. The green area ranges from −162‰ to −110‰ represents freshwater origin and the blue area ranges from −212‰ to −134‰ represents freshwater origin, the intermediate turquoise area represents the freshwater and saltwater transition environment.

5.1.2. Parent Material Origin Comparison

The max carbon peak (Nmax), higher plant input parameter (TAR), *n*-C_{21}-/*n*-C_{22} +, (*n*-C_{21} + *n*-C_{22})/(*n*-C_{28} + *n*-C_{29}), 2*n*-C_{17}/(*n*-C_{23} + *n*-C_{25}), and CPI and OEP can be used to reflect the distribution characteristics of n-alkanes and the parent material origin of source rocks [39,40]. According to these parameter results, the Es_3 source rock has the characteristics of mixed-source organic, with both higher plants and lower aquatic organisms, such as algae. The relevant parameter results of the crude oil samples also reflect that the parent material is mixed-source input.

The oleanane (Ol) is a dating marker of tertiary organic matter, mainly derived from triterpenoids in angiosperms [41]. Based on the results, the Ol/C_{30}H ratio of the Es_3 source rocks is 0.082~0.103, indicating a certain amount of higher plant input. Meanwhile, the crude oils also show a lower Ol/C_{30}H ratio and have a good correlation with the Es_3 source rocks (Figure 6).

C_{19} tricyclic terpane (C_{19}TT), C_{20} tricyclic terpane (C_{20}TT), and C_{24} tricyclic terpane (C_{24}TT) are abundant in crude oil, with more input from terrigenous higher plants [42]. C_{23}TT indicates the input of lower aquatic organisms [34], and long-chain tricyclic terpenes of C_{28}TT and C_{29}TT are mainly derived from the green algae and bacteria [33]. According to the results of related parameters (Table 2), it can be inferred that Es_3 had a mixed-source input, with higher plants, algae, and bacteria accounting for a certain proportion. Regarding the oil-source correlation according to the C_{19}TT/C_{23}TT and ETR values of the source rock and crude oil samples (Figure 10), the crude oils and the Es_3 source rocks have a high distribution similarity in the same area, indicating that the crude oils are most likely to be generated by the Es_3 source rock.

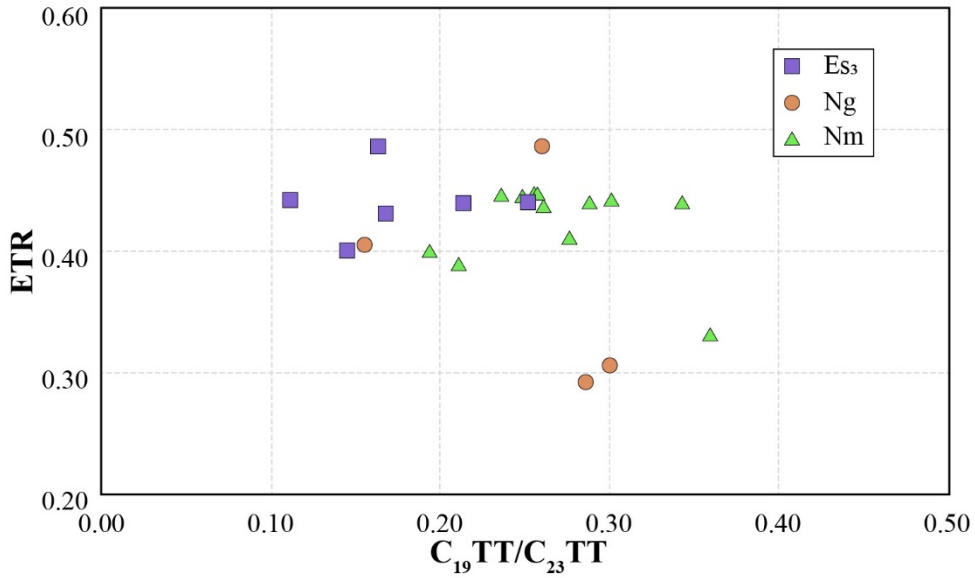


Figure 10. Relation between $C_{19}TT/C_{23}TT$ ratio and ETR.

For the C_{27}, C_{28}, and C_{29} conventional steranes, the content of $C_{29}S$ is correlated with the input of higher plants, and the relative content of $C_{27}S$ and $C_{28}S$ is correlated with the input of aquatic organisms, such as algae [43,44]. From the ternary diagram (Figure 11) of the C_{27}, C_{28}, and C_{29} conventional steranes, the parent material of the Es_3 source rocks is mainly a mixed source with both terrigenous higher plants and phytoplankton. The distribution of crude oils' conventional steranes is limited and similar to that of Es_3 source rocks, indicating that the oil parent material origin is also mixed with phytoplankton as the main source.

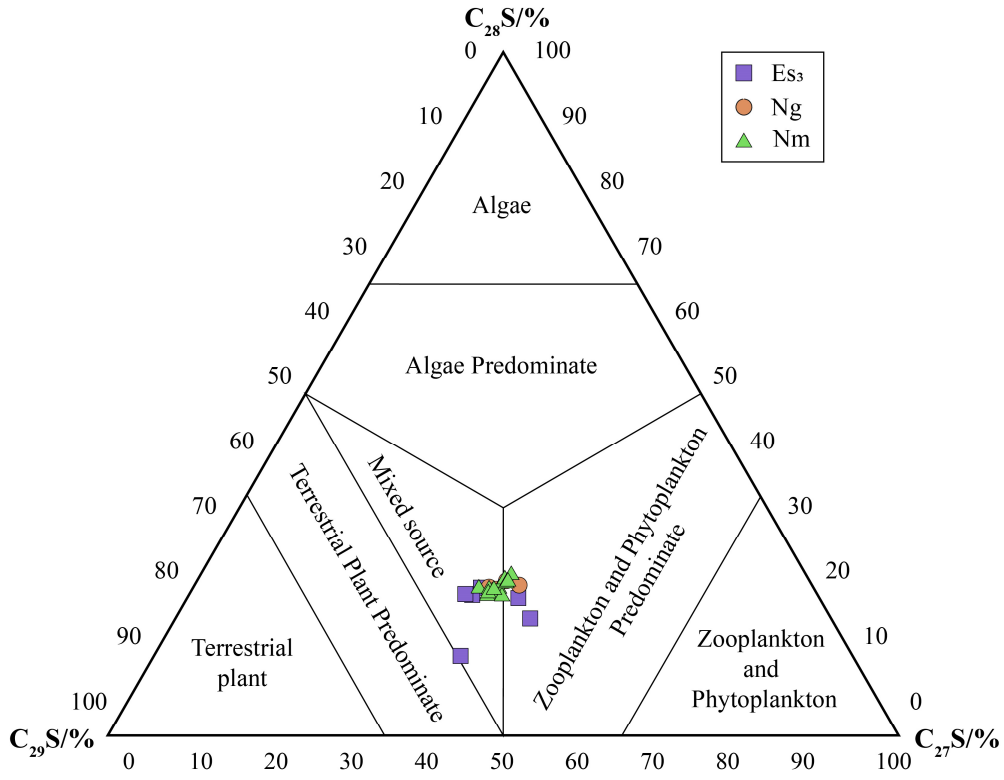


Figure 11. Ternary diagram of the relative percentages of C_{27}, C_{28}, and C_{29} steranes.

Specific differences exist in the n-alkanes carbon isotopes formed by aquatic and terrestrial organisms. The n-alkanes of aquatic organisms are rich in the light carbon isotope, while the n-alkanes of terrestrial organisms are rich in the heavy carbon isotope, which may be due to the different carbon sources used by aquatic organisms and terrestrial organisms [45,46] (Figure 8). The carbon isotope values of saturated hydrocarbon monomers show a trend of higher on the left and lower on the right. The long-chain *n*-C_{32} and *n*-C_{34} also present higher carbon isotope values, indicating that the parent material of the crude oil samples also has the contribution of terrigenous organisms. In summary, crude oil as a whole is a mixed-source input.

5.1.3. Thermal Maturity Comparison

C_{30}H and Tm are rearranged to form C_{30} diahopane (C_{30}diaH) and Ts, with the thermal evolution degree increasing [21]. According to the GC-MS results, C_{30}diaH exists in both the Es_3 source rocks and the crude oils. The Es_3 source rocks have high Ts/Tm values similar to those of the crude oil samples. Meanwhile, the C_{30}diaH/C_{30}H and Ts/Tm values of the Es_3 source rocks and crude oils were plotted in the same area (Figure 12), indicating that the Es_3 source rocks have a good correlation with Neogene crude oils.

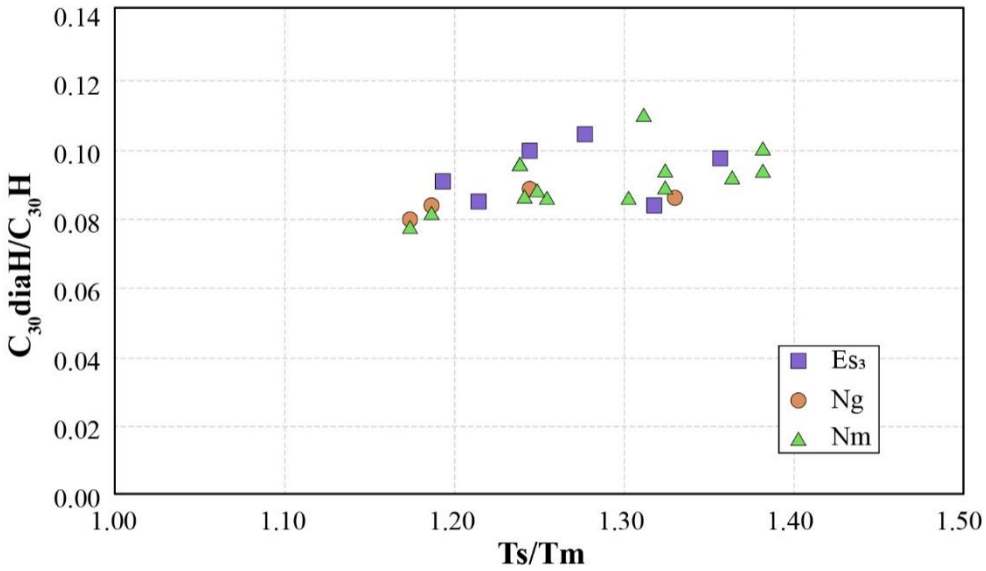


Figure 12. Biomarker maturity indicators of C_{30}diaH/C_{30}H and Ts/Tm ratios.

With the increasing thermal evolution degree, part of C_{29} hopane (C_{29}H) will gradually be rearranged to form C_{29}Ts, and the 22R configuration of homohopane will also gradually be transformed to the mixture of the 22S and 22R configurations, and finally reach equilibrium [21]. The Es_3 source rock samples have a high C_{29}Ts/C_{29}H and 22S/(22S + 22R) ratio of C_{31} to C_{35} homohopanes (%22S) similar to those of the crude oil samples, confirming the affinity between them. The thermal maturity of the source rocks can be described by the values of %20S and %ββ, which are 0.35~0.4 and 0.36~0.46, respectively. R_o should be in the oil window range (0.5%~1.3%) [39].

Similar to the above maturity biomarkers, the 20S and ββ configurations of the conventional steranes and C_{27} diasteranes (C_{27}diaS) gradually increase their contents to equilibrium, with thermal evolution increasing, so their relevant parameters can be used to reflect the maturity of the source rocks and crude oils. The average C_{27}diaS/C_{27}S value of the Es_3 source rock samples is 0.29, while that of the crude oil samples is 0.25, indicating a good correlation between the two. The average %20S of the Es_3 source rocks and crude oils is 0.44 and 0.41, respectively. The ββ/(αα + ββ) isomerization of the C_{29} 20S and 20R regular steranes (%ββ) mean value of the Es_3 source rocks and crude oil samples is 0.40 and 0.44, respectively. From the two parameters of the 20S/(20S + 20R) ratio of C_{29}ααα

sterane (%20S) and %ββ (Figure 13), most of the crude oil samples are distributed in the same area, which is basically in the same range as the Es_3 source rocks.

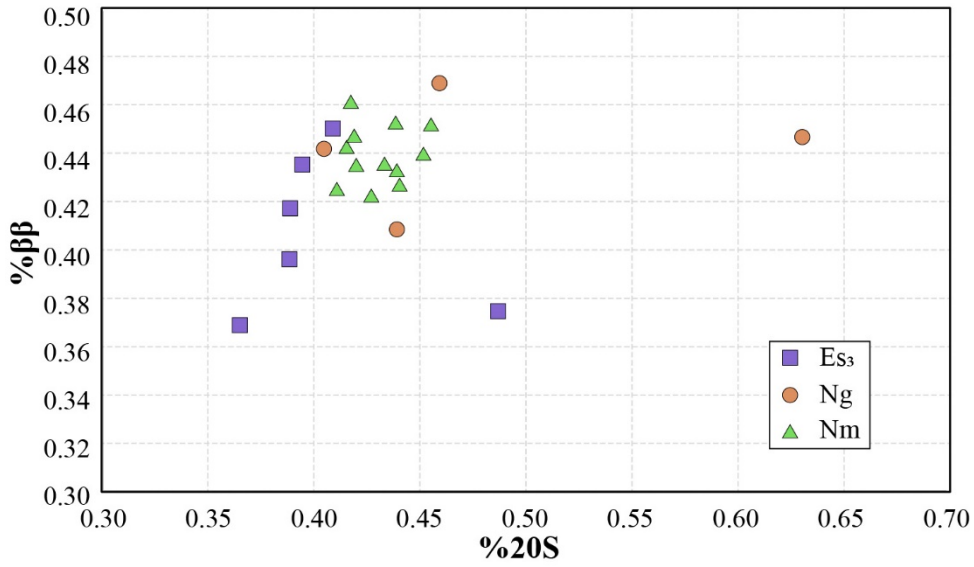


Figure 13. Characteristics of C_{29} sterane isomerization parameters of hydrocarbon source rocks and crude oils.

Overall, the crude oils and the Es_3 source rocks have a similar maturity with biomarker parameters. Therefore, this observation provides an additional line of evidence that the Neogene oils originated from the Es_3 source rock.

5.2. Possibility of Hydrocarbon Supply from Other Source Rocks

Previous studies confirmed that the Es_3 Source rocks are also the primary source rocks in other adjacent depressions (sags), such as the Chengbei sag, Bozhong depression, Bodong sag, and Miaoxi sag [47–53]. The depositional environment and parent material of the Es_3 source rock in the surrounding depression (sag) are similar to those in the Huanghekou sag. The Es_3 gammacerane content in the Bozhong depression is low [47–49], and the $Ga/C_{30}H$ values range from 0.03 to 0.07, with an average value of 0.05. The Es_3 $Ga/C_{30}H$ ratio is also not high in the Bodong sag, with values between 0.14 and 0.21 [50], the Chengbei sag less than 0.20 [51], and the Miaoxi sag less than 0.15 [52]. The low gammacerane content reflects a brackish water sedimentary environment, similar to that in the middle Huanghekou sag. Except for this, Pr/Ph, C_{19}/C_{23} tricyclic terpane, and other Es_3 biomarker parameters in these surrounding depressions (sag) also have similar values as the middle Huanghekou sag, reflecting the Es_3 sedimentary environment of weak reduction to weak oxidation and characteristics of the mixed source.

In addition to the Es_3 source rocks, the Es_4 strata developed in some surrounding depressions (sags). Further, they are considered as good hydrocarbon source rocks, such as southern Miaoxi sag, eastern Huanghekou sag, Dongying sag, etc. [36,53]. High-sulfur oil reservoirs were also found in the eastern Huanghekou sag and the northeastern part of the Laizhou Bay sag, which had the characteristics of lower Pr/Ph and higher $Ga/C_{30}H$ [54]. These high-sulfur crude oils were proved to come from the Es_4 source rocks, which were carbonate-rich and deposited under a saline anoxic environment [54]. At the same time, the Es_4 gammacerane content is very high. For example, the $Ga/C_{30}H$ ratio in the Dongying sag ranges from 0.44 to 1.88, with an average value of 1.26 [37]. The Pr/Ph values are all less than 0.5, reflecting the strong reducing and saltwater sedimentary environment, indicating that the Es_4 formation deposited in a marine sedimentary environment completely different from the Es_3 delta sedimentary environment.

Combined with the comparison of the source rocks and Neogene oils, the relevant Es_3 biomarker parameters in the middle Huanghekou sag are similar to those in the surrounding sags. In contrast, the biomarker characteristics of the Es_4 and Es_3 source rocks are quite different, which is also inconsistent with the characteristics of the Neogene crude oil in the middle Huanghekou sag. Therefore, the possibility of the Es_4 formation being the regional source rock for the Neogene crude oil can be ruled out. It is further inferred that the middle Huanghekou sag lacks the sedimentation of the Es_4 formation.

6. Conclusions

Through the study of the oil-source correlation of the Paleogene source rock and Neogene crude oil in the middle Huanghekou sag, we determined the Neogene crude oils have a good correlation with the mature Es_3 source rocks. The Es_3 sedimentary environment is a brackish or a freshwater delta deposition under weak oxidation–weak reduction conditions, reflected by the biomarkers and carbon and hydrogen isotopes of the saturated hydrocarbon monomers of the crude oil and source rock. The Es_3 parent material comes from the mixed-source input of terrigenous higher plants and phytoplankton. There is a significant difference in biomarkers between the Neogene crude oils in the middle Huanghekou sag and the Es_4 source rock in the surrounding depression (sags), reflecting the Es_4 sedimentation absence in the study sag. In recent years, shallow Neogene oil reservoirs have been discovered and distributed around the hydrocarbon generation sag. Oil and gas exploration should also focus on the Es_3 hydrocarbon generation center to find suitable lithological and structural traps in the future.

Author Contributions: Conceptualization, R.H. and X.L.; methodology, R.H.; formal analysis, R.H. and X.L.; writing—original draft preparation, R.H.; writing—review and editing, R.H. and X.L.; funding acquisition, H.L. All authors have read and agreed to the published version of the manuscript.

Funding: This research was funded by National Science and Technology Major Project (2016ZX05024-003-003) and the APC was funded by China University of Geosciences, Beijing.

Data Availability Statement: The data presented in this study are available on request from the corresponding author.

Acknowledgments: The authors would like to thank the National Science and Technology Major Project (2016ZX05024-003-003) for its support.

Conflicts of Interest: The authors declare no conflict of interest.

References

1. Qi, J.F.; Yang, Q. Neogene structural deformation and dynamic processes of the Bohai Bay basin province, China. *Mar. Petrol. Geol.* **2010**, *27*, 757–771. [CrossRef]
2. Xu, S.; Hao, F.; Xu, C.G.; Wang, Y.B.; Zou, H.Y.; Gong, C.L. Differential compaction faults and their implications for fluid expulsion in the northern Bozhong Subbasin, Bohai Bay Basin, China. *Mar. Petrol. Geol.* **2015**, *63*, 1–16. [CrossRef]
3. Qiu, N.S.; Xu, W.; Zuo, Y.H.; Chang, J. Meso-Neogene thermal regime in the bohai Bay Basin, eastern north China craton. *Int. Geol. Rev.* **2015**, *57*, 271–289. [CrossRef]
4. Hao, F.; Zou, H.Y.; Gong, Z.S.; Deng, Y.H. Petroleum migration and accumulation in the Bozhong sub-basin, Bohai Bay basin, China: Significance of preferential petroleum migration pathways (PPMP) for the formation of large oilfields in lacustrine fault basins. *Mar. Petrol. Geol.* **2007**, *24*, 1–13. [CrossRef]
5. Hao, F.; Zhou, X.H.; Zhu, Y.M.; Zou, H.Y.; Bao, X.H.; Kong, Q.Y. Mechanisms of petroleum accumulation in the Bozhong sub-basin, Bohai Bay basin, China. Part 1: Origin and occurrence of crude oils. *Mar. Petrol. Geol.* **2009**, *26*, 1528–1542. [CrossRef]
6. Hao, F.; Zhou, X.H.; Zhu, Y.M.; Yang, Y.Y. Lacustrine source rock deposition in response to co-evolution of environments and organisms controlled by tectonic subsidence and climate, Bohai Bay Basin, China. *Org. Geochem.* **2011**, *42*, 323–339. [CrossRef]
7. Chen, B.; Deng, Y.H.; Hao, F.; Zou, H.Y.; Hu, J.W. Late-stage rapid petroleum accumulation model of BZ34 fault zone in Huanghekou Sag. *Acta. Petrol. Sin.* **2006**, *27*, 37–41. (In Chinese with English Abstract)
8. Xue, Y.A.; Yang, H.F.; Xu, C.G. Differential reservoir-controlling effect and hydrocarbon enrichment of slope zone in Huanghekou sag, Bohai Bay Basin. *China Petrol. Explor.* **2016**, *21*, 65–74. (In Chinese with English Abstract)
9. Xu, C.G.; Yu, H.B.; Wang, J.; Liu, X.J. Formation conditions and accumulation characteristics of Bozhong 19-6 large condensate gas field in offshore Bohai Bay Basin. *Petrol. Explor.* **2019**, *46*, 27–40. [CrossRef]

10. Xu, H.Y.; George, S.C.; Hou, D.J. The occurrence of isorenieratane and 24-npropylcholestanes in Paleogene lacustrine source rocks from the Dongying Depression, Bohai Bay Basin: Implications for bacterial sulfate reduction, photic zone euxinia and seawater incursions. *Org. Geochem.* **2019**, *127*, 59–80. [CrossRef]
11. Guo, T.; Yang, B.; Chen, L.; Yang, H.F.; Wang, X.Y.; Liu, Q.S.; Tu, X. 3d fine description of magmatic rocks: The discovery of BZ34-9 oil field in the southern slope of Huanghekou sag. *China Offshore Oil and Gas* **2016**, *28*, 71–77. (In Chinese with English Abstract)
12. Yang, H.F.; Niu, C.M.; Liu, Y.J.; Gao, Y.F.; Zhang, Z.Q.; Xie, X.; Wang, L.L. Discovery and key exploration technology of KL6-1 large lithologic oil reservoir of Neogene in the Bohai Bay Basin. *China Petrol Explor.* **2020**, *25*, 24–32. (In Chinese with English Abstract)
13. Xu, C.G.; Yang, H.F.; Wang, D.Y.; Zhao, D.J.; Wang, L.L. Formation conditions of Neogene large-scale high-abundance lithologic reservoir in the Laibei low uplift, Bohai Sea, East China. *Petrol. Explor. Dev.* **2021**, *48*, 12–25. (In Chinese with English Abstract) [CrossRef]
14. Liu, H.; Xia, Q.L.; Somerville, L.D.; Wang, Y.; Zhou, X.H.; Niu, C.M.; Du, X.F.; Zhang, X.T. Paleogene of the Huanghekou Sag in the Bohai Bay Basin, NE China: Deposition-erosion response to a slope break system of rift lacustrine basins. *Geol. J.* **2015**, *50*, 71–92. [CrossRef]
15. Hao, F. *Hydrocarbon Generation Kinetics and Hydrocarbon Accumulation Mechanism in the Overpressured Basin*; China Social Sciences Press: Beijing, China, 2005.
16. Li, J.P.; Xin, R.C.; Xiang, S.M.; Guo, T. Sedimentary characteristics of the Member3 of Paleogene Dongying Formation in Huanghekou Sag, Bohai Bay Basin. *J. Palaeogeogr.* **2008**, *10*, 363–370. (In Chinese with English Abstract)
17. Sun, H.F.; Zhou, X.H.; Peng, W.X.; Zou, H.Y.; Yang, B.; He, D.B.; Zeng, X. Late-stage hydrocarbon accumulation and enrichment in the Huanghekou Sag, southern Bohai Sea. *Petrol. Explor. Dev.* **2011**, *38*, 307–313. (In Chinese with English Abstract)
18. Yang, H.F.; Xu, C.G.; Niu, C.M.; Qian, G.; Li, Z.Y.; Gao, Y.F.; Huang, Z. Quantitative evaluation of hydrocarbon accumulation pattern and the controlling factors in the Neogene of Huanghekou Sag, Bohai Bay Basin. *Oil Gas Geol.* **2020**, *41*, 259–269. (In Chinese with English Abstract)
19. Wang, S.; Wang, F.L.; Chen, R.T.; Cheng, F.Q.; Liu, M.X. Organic Geochemical Characteristics of Source Rocks in Huanghekou Sag. *J. Xi'an Shiyou Univ.* **2022**, *37*, 9–15+26. (In Chinese with English Abstract)
20. Volkman, J.K. Biological marker compounds as indicators of the depositional environments of petroleum source rocks. *Geol. Soc. Lond. Spec. Publ.* **1988**, *40*, 103–122. [CrossRef]
21. Peters, K.E.; Moldowan, J.M. *The Biomarker Guide: Interpreting Molecular Fossils in Petroleum and Ancient Sediments*; Prentice-Hall, Inc.: Englewood Cliffs, NJ, USA, 1993.
22. Andrew, P.M.; Roger, E.S.; Christopher, J.B.; Lesley, M.D. Biomarker and n-alkane isotope profiles for Tertiary oils: Relationship to source rock depositional setting. *Org. Geochem.* **1994**, *22*, 521–542.
23. Christopher, J.B.; Roger, E.S.; Roksandic, Z.; Lesley, M.D.; Adrian, C.H. Chemical, molecular and isotopic differentiation of organic facies in the Tertiary lacustrine Duaringa oil shale deposit, Queensland, Australia. *Org. Geochem.* **1994**, *21*, 685–712.
24. Clayton, C.J.; Bjory, M. Effect of maturity on ratios of individual compounds in North Sea oils. *Org. Geochem.* **1994**, *21*, 737–750. [CrossRef]
25. Li, M.W.; Huang, Y.S.; Obermajer, M.; Jiang, C.Q.; Lloyd, R.S.; Martin, G.F. Hydrogen isotopic compositions of individual alkanes as a new approach to petroleum correlation: Case studies from the western Canada sedimentary basin. *Org. Geochem.* **2001**, *32*, 1387–1399. [CrossRef]
26. Tissot, B.P.; Welte, D.H. *Petroleum Formation and Occurrence*; Springer: New York, NY, USA, 1984; pp. 258–266.
27. Philp, R.P.; Gilbert, T.D. Biomarker distributions in Australian oils predominantly derived from terrigenous source material. *Org. Geochem.* **1986**, *10*, 73–84. [CrossRef]
28. Chen, X.Y.; Hao, F.; Guo, L.X.; Wang, D.J.; Yin, J.; Yang, F.; Zou, H.Y. Origin of petroleum accumulation in the Chaheji-Gaojiapu structural belt of the Baxian Sag, Bohai Bay Basin, China: Insights from biomarker and geological analyses. *Mar. Petrol. Geol.* **2018**, *93*, 1–13. [CrossRef]
29. Alexander, R.; Kagi, R.I.; Woodhouse, G.W. Geochemical correlation of windalia oil and extracts of winning group (cretaceous) potential source rocks, barrow subbasin, western Australia. *AAPG Bull.* **1981**, *65*, 235–250.
30. Peters, K.E.; Cunningham, A.E.; Walters, C.C.; Jiang, J.G.; Fan, Z.A. Petroleum systems in the jiangling-dangyang area, jianghan basin, China. *Org. Geochem.* **1996**, *24*, 1035–1060. [CrossRef]
31. Moldowan, J.M.; Seifert, W.K.; Gallegos, E.J. Relationship between petroleum composition and depositional environment of petroleum source rocks. *AAPG Bull.* **1985**, *69*, 1255–1268.
32. Tian, J.Q.; Hao, F.; Zhou, X.H.; Zou, H.Y.; Lan, L. Charging of the Penglai9-1 oil field, Bohai Bay basin, China: Functions of the delta on accumulating petroleum. *Mar. Petrol. Geol.* **2014**, *57*, 603–618. [CrossRef]
33. Wang, Q.; Hao, F.; Xu, C.G.; Wang, Y.B.; Zou, H.Y. Geochemical characterization of QHD29 oils on the eastern margin of Shijiutuo uplift, Bohai Sea, China: Insights from biomarker and stable carbon isotope analysis. *Mar. Petrol. Geol.* **2015**, *64*, 266–275. [CrossRef]
34. Barnes, M.A.; Barbers, W.C. Oxic and anoxic diagenesis of diterpenes in lacustrine sediments. In *Advances in Organic Geochemistry 1981*; Bjorøy, M., Albrecht, C., Cornford, C., Eds.; John Wiley & Sons: New York, NY, USA, 1983; pp. 289–298.
35. Aquino Neto, F.R.; Trendel, J.M.; Restl'e, A.; Connan, J.; Albrecht, P.A. Occurrence and formation of tricyclic terpanes in sediments and petroleums. In *Advances in Organic Geochemistry 1981*; John Wiley & Sons: New York, NY, USA, 1983; pp. 659–667.

36. Li, S.M.; Pang, X.Q.; Jiang, Z.X.; Qiu, G.Q.; Gao, Y.J. Quantitive predication and significance of mixed oils for lithologic oil pool in the Dongying Depression of the Bohai Bay Basin. *Petrol. Geol Exp.* **2009**, *31*, 262–269. (In Chinese with English Abstract)
37. Li, S.M.; Guo, D. Characteristics and Application of Compound Specific Isotope in Oil-source Identification for Oils in Dongying Depression, Bohai Bay Basin. *Geoscience* **2010**, *24*, 252–258. (In Chinese with English Abstract)
38. Qi, Y.L. Method and application of hydrogen isotope analysis of n-alkanes. *Petrol. Geol. Exp.* **2020**, *42*, 319–324. (In Chinese with English Abstract)
39. Seifert, W.K.; Moldowan, J.M. Use of biological markers in petroleum exploration. *Methods. Geochem. Geophys.* **1986**, *24*, 261–290.
40. Gelpi, E.; Schneider, H.; Mann, J.; Oro, J. Hydrocarbons of geochemical significance in microscopic algae. *Phytochem.* **1970**, *9*, 603–612. [CrossRef]
41. Moldowan, J.M.; Dahl, J.; Huizinga, B.J.; Fago, F.J.; Hickey, L.J.; Peakman, T.M.; Taylor, D.W. The molecular fossil record of oleanane and its relation to angiosperms. *Science* **1994**, *265*, 768–771. [CrossRef]
42. James, E.S.; Claire, L.S. Saturated hydrocarbons in the sediments of Lake Apopka, Florida. *Org. Geochem.* **2003**, *34*, 253–260.
43. Patterson, G.W. The distribution of sterols in algae. *Lipids* **1971**, *6*, 120–127. [CrossRef]
44. Grantham, P.J. The occurrence of unusual C_{27} and C_{29} sterane predominances in two types of Oman crude oil. *Org. Geochem.* **1986**, *9*, 1–10. [CrossRef]
45. Stahl, W.J. Carbon and nitrogen isotopes in hydrocarbon research and exploration. *Chem. Geol.* **1977**, *20*, 121–149. [CrossRef]
46. Hayes, J.M. Factors controlling ^{13}C contents of sedimentary organic compounds: Principles and evidence. *Mar. Geol.* **1993**, *113*, 111–125. [CrossRef]
47. Huang, X.; Yang, H.F.; Wang, L.F.; Xu, Y.H.; Tang, G.M.; Wang, N. Sedimentary environment and formation mechanism of organic-rich mudstone in the third member of Shahejie Formation in the southwestern Bozhong Sag, Bohai Bay Basin. *Nat. Gas. Geosci.* **2022**, *33*, 2032–2048. (In Chinese with English Abstract)
48. Huang, Q.; Chen, R.T.; Peng, X.B.; Li, X.Q.; Wang, N. Characteristics and geological significance of biomarkers from the Paleogene source rocks in Bozhong Sag. Bohai Bay Basin. *Bull. Geol. Sci. Technol.* **2022**, *41*, 180–192. (In Chinese with English Abstract)
49. Li, G.X.; Liu, C.L.; Wang, F.L.; Tang, G.M.; Yang, H.; Zeng, X.X.; Wu, Y.P.; Yang, X.Y. Geochemical characteristic sand hydrocarbon generation mode of source rocks of Dongying Formation in Bozhong sag, Bohai Bay Basin. *Acta. Petrol. Sin.* **2022**, *43*, 1568–1584. (In Chinese with English Abstract)
50. Li, C.Z.; Xu, F.H.; Huang, X.B.; Jiang, T.; Xu, G.S.; Guo, P. Migration directions of crude oils from multiple source rock intervals based on biomarkers: A case study of Neogene reservoirs in the Bodong Sag, Bohai Bay Basin. *Energy Rep.* **2022**, *8*, 8151–8164. [CrossRef]
51. Li, C.G.; Zhou, Y.H. The main petroleum system description of the east section of south slope of Chengbei sag. *Nat. Gas Geosci.* **2000**, *11*, 26–29. (In Chinese with English Abstract)
52. Jia, N.; Liu, C.Y.; Zhang, D.D. Study on hydrocarbon source rock characteristics and oil-source correlation in Miaoxi Depression, Bohaiwan Basin. *J. Northwest Univ.* **2013**, *43*, 461–465. (In Chinese with English Abstract)
53. Liu, D.D.; Tang, G.M.; Wang, F.L. Characteristics of Hydrocarbon Source Rocks and Analysis of Oil Source in Eastern Sag of Bohai Sea Area. *J. Xi'an Shiyou Univ.* **2020**, *35*, 9–17+27. (In Chinese with English Abstract)
54. Niu, C.K.; Hou, D.J.; Cheng, X.; Han, X.; Li, Y.X. Origin and environmental implications of dibenzothiophenes in the Huanghekou East Sag and the Laizhouwan Northeast Sag, Bohai Bay Basin. *Mar. Petrol. Geol.* **2022**, *142*, 105739. [CrossRef]

Disclaimer/Publisher's Note: The statements, opinions and data contained in all publications are solely those of the individual author(s) and contributor(s) and not of MDPI and/or the editor(s). MDPI and/or the editor(s) disclaim responsibility for any injury to people or property resulting from any ideas, methods, instructions or products referred to in the content.